Analytica Chimica Acta 1211 (2022) 339904

Contents lists available at ScienceDirect

Analytica Chimica Acta

journal homepage: www.elsevier.com/locate/aca

Nanobody-based label-free photoelectrochemical immunoassay for highly sensitive detection of SARS-CoV-2 spike protein

Yun Chen [a], Wei Duan [a], Li Xu [a], Guanghui Li [b], Yakun Wan [b,**], Henan Li [a,*]

[a] School of Chemistry and Chemical Engineering, Institute for Energy Research, Jiangsu University, Zhenjiang, 212013, China
[b] Shanghai Novamab Biopharmaceuticals Co., Ltd., Shanghai, 201318, China

HIGHLIGHTS

- Au@TiO_2 nanomaterial exhibited superior PEC performance owing to SPR effect of Au.
- Nanobody was well incubated by the formed conjugates with Au@TiO_2.
- The PEC immunoassay realized highly sensitive detection for SARS-CoV-2 spike protein.

GRAPHICAL ABSTRACT

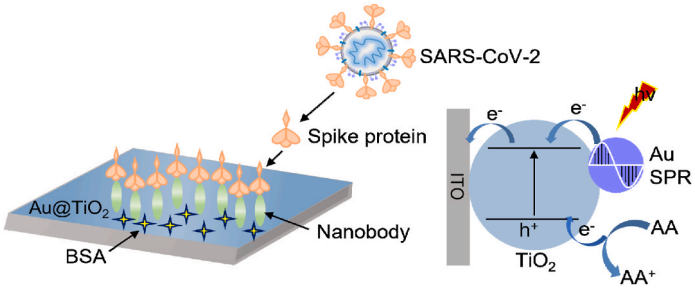

ARTICLE INFO

Keywords:
SARS-CoV-2
Spike protein
Immunoassay
Photoelectrochemical
Nanobody

ABSTRACT

Until now, COVID-19 caused by SARS-CoV-2 is engulfing the worldwide and still ranging to date, continuing to threaten the public health. The main challenge facing COVID-19 epidemic is short of fast-response and high-efficiency methods to determine SARS-CoV-2 viral pathogens. Herein, a nanobody-based label-free photoelectrochemical (PEC) immunosensor has been fabricated for rapidly detecting SARS-CoV-2 spike protein. As a small-size and high-stability antibody, nanobody was directly and well immobilized with Au nanoparticles and TiO_2 spheres by the interaction. Au deposited TiO_2 nanomaterial possessed 8.5 times photoelectric performance in comparison with TiO_2 in the presence of electron donor owing to surface plasma resonance effect of Au. Based on the steric hindrance effect, this immunoassay platform realized the linear detection from 0.015 to 15000 pg mL^{-1}, and a limit of detection was low as 5 fg mL^{-1}. The label-free PEC immunoassay design provides a new idea for convenient, rapid, and efficient test of SARS-CoV-2 spike protein and broadens further application of nanobody as an identification agent to specific biomarkers.

1. Introduction

Coronavirus disease (COVID-19) has caused the global outbreak with millions of deaths, and the death toll is still rising. Severe acute respiratory syndrome coronavirus type 2 (SARS-CoV-2) is the pathogen of COVID-19, which has an envelope structure and contains genetic substrate of single positive-stranded RNA [1–3]. The virus is a β coronavirus derived from bats, and phylogenetic studies have shown that it

** Corresponding author.
* Corresponding author.
E-mail addresses: ykwan@novamab.com (Y. Wan), lhn@ujs.edu.cn (H. Li).

https://doi.org/10.1016/j.aca.2022.339904
Received 22 February 2022; Received in revised form 29 April 2022; Accepted 1 May 2022
Available online 3 May 2022

may infect humans and spread among human hosts through other intermediate hosts [4]. Test technologies such as reverse transcription polymerase chain reaction (RT-PCR), computed tomography (CT) scan, and immunoassay are on the rise to achieve the monitoring of COVID-19. RT-PCR test takes relatively long time for analysis (minimum of 3 h) and requires several complicated steps. Moreover, RT-PCR is relatively expensive which hindered its wide applicability for population scale diagnosis of SARS-CoV-2, particularly in low and middle-income countries [5,6]. CT scan of the chest is sensitive, painless, and non-invasive routine test, especially in the early stages. However, it requires expensive equipment with technical experts to operate it, and as the chest abnormalities are like to those of other viral cases of pneumonia, it cannot selectively diagnose COVID-19 [7]. Immunoassay can give a better insight into the actual COVID-19 infection level of the population and be also implemented to identify the presence of corresponding antigens in COVID-19 patients [8,9]. It does not require special laboratory equipment, highly trained personnel, or specific reagents. Sensitive, rapid, and accurate diagnostic methods based on the direct detection of the viral antigen without pretreatment are highly demanded to control COVID-19 outbreak. Therefore, compared with RT-PCR and CT tests, immunoassay is cost-effective for both mass production and administration. In the body of patients, the highly expressed angiotensin-converting enzyme 2 (ACE2) binds to spike (S) protein on the envelope of SARS-CoV-2 [10–12], seriously threatening the safety of people and impeding normal operation of the world. As COVID-19 is strong infectivity and lethality, and large number of patients continue to increase, it is imperative to massively screen the entire population for S protein of SARS-CoV-2.

Immunoassay is a biochemical and rapidly developed method for quantitative or qualitative determination of specific biomarkers using the immunoreaction between antigen and antibody [12]. The accuracy and operability of immunoassay promote the rapid development for biological analysis, clinical medicine, food safety, and environmental monitoring [13,14]. The labelled immunosensor utilize the combination of detectable labels with antibody or antigen. Labels such as chromophores, fluorophores, and enzymes are typically linked or conjugated to the desired antibodies or antigens. There are labelled immunoassays such as electrochemical sensors [10,12,15,16], surface-enhanced Raman scattering-based immunodiagnostic sensor [17], and single-walled carbon nanotube-based optical sensing [18], achieving for the monitoring of SARS-CoV-2 S protein. But it may be limited in a higher cost and more complicated device than the label-free sensor. The label-free immunoassay system usually correlates to the steric hindrance effect produced by the immunoreaction of antigen and antibody. Its structure is relatively simple, which can significantly reduce the assay time, the amount of chemical consumption, and the overall assay costs [19]. Photoelectrochemical (PEC) immunosensor possesses these advantages including fast response, high sensitivity, high selectivity, and reduced or even negligible background affect [20,21]. In the label-free PEC immunoassay system, target antigen captured on the electrode substrate with the immobilized antibody causes the increase of steric effect, which hinders the diffusion of photoinduced charges to the conductive matrix and reduces the photocurrent signal, allowing for the sensitive detection of antigen. It is worth noting that there is no report about the use of label-free PEC immunosensor to monitor S protein of SARS-CoV-2.

A unique antibody fragment, called nanobody (Nb, ~2.5 × 3 × 4 nm) [22] or variable domain of heavy chain of heavy chain antibody (VHH) [23], is the smallest known antibody molecule of binding antigen in size (~15 kDa) [24,25]. Nb has small molecular weight, simple structure, easy cloning or genetic modification and can be expressed in large quantities in microbial expression systems [26]. Notably, VHH antibody can efficiently bind to antigen (nanomolar or even picomolar level) due to highly chemical properties and possesses high affinity [27–29]. As a structural domain with only one intrachain disulfide bond compared with conventional antibody, its structure is relatively stable (the resistance of high temperature, acid, and alkali). For example, it can maintain high antigen binding ability after being placed at 37 °C for several weeks, and even tolerating high temperature (60–80 °C) [30]. Nb with the small size can be well coupled to a higher density on the PEC immunosensor to raise signal-to-noise ratio than that of conventional antibody [31], thereby reducing limit of detection (LOD) and realizing sensitive analysis for antigen. Inspired by the above-mentioned advantages, a Nb-based PEC immunoassay was designed and utilized for the label-free detection of SARS-CoV-2 S protein. Considering surface plasma resonance (SPR) effect of Au nanoparticles, Au@TiO_2 nanomaterial possessed excellent photoelectric performance in contrast to single TiO_2. Nb was effectively anchored by the formation of the conjugates between Nb and Au@TiO_2 photoactive material. This prepared Nb-based PEC immunoassay of S protein has realized the sensitive (LOD: ~5 fg mL^{-1}) and stable analysis.

2. Experimental section

2.1. Reagents and apparatus

Titanium butoxide (TBOT, ≥99.0%) and ammonia solution (25.0–28.0%) were obtained from Shanghai Aladdin Biochemical Technology and Kunshan Reagent, respectively. Trisodium citrate dihydrate ($C_6H_5Na_3O_7·H_2O$, ≥99.0%), L-ascorbic acid (AA, ≥99.7%), ethanol absolute (EtOH), and tetrachloroauric(III) acid tetrahydrate ($HAuCl_4·4H_2O$) were purchased from Sinopharm. Bovine serum albumin (BSA) and phosphate buffered saline (PBS, 6.7 mmol L^{-1}, pH 7.4) were bought from Hyclone Laboratory of the USA. During all experiments, ultrapure water (H_2O, 18.25 MΩ cm) was purified by Sichuan ULUPURE Instrument. Nb and S protein were selected and purified by the reported literature (Novamab Biopharmaceuticals Co., Ltd.), where the selectivity and affinity have been verified by Gai et al. [32]. The purchased Nb was configured and diluted into the solution separately. Briefly, thaw it from −20 °C to 4 °C, followed by centrifugation and oscillating for 30 min into the bottom. Afterwards, certain PBS (6.7 mmol L^{-1}, pH 7.4) was slowly added to obtain certain concentration, continuing to oscillate for another 30 min. Finally, the treated Nb solution was packaged by multi-tube and stored in the refrigerator of 4 °C for later measurement.

An XRD-6100 Lab X-ray diffractometer (Shimadzu, Japan) was performed for X-ray powder diffraction (XRD) testing with Cu Kα radiation at a scan rate of 7° min^{-1}. JSM-7800F microscopy (JEOL, Japan) was employed for scanning electron microscopy (SEM) analysis. JEM-2010F microscopy (JEOL, Japan) was adopted for high-resolution transmission electron microscopy (HRTEM) characterization. UV-2600 spectroscopy (Shimadzu, Japan) was conducted for ultraviolet–visible diffuse reflectance spectra (DRS) collection. Both photocurrent signal and electrochemical impedance spectroscopy (EIS) measurement were implemented by CHI660E electrochemical workstation (Shanghai CH Instrument Co., Ltd.) under a representative three-electrode system, where Ag/AgCl (Shanghai CH Instrument, CHI111, a potential of 0 V), Pt wire (Shanghai CH Instrument, CHI115) and indium tin oxide (ITO, Kaivo Optoelectronic Technology) were acted as reference, counter and working electrode, respectively. Transient photocurrent response was tested in PBS with the addition of 0.1 mol L^{-1} AA. High uniformity integrated Xenon light with the wavelength range from 320 nm to 780 nm (300 W, PLS-FX300HU, Beijing Perfectlight) was used as exciting light source. EIS analysis was operated at the frequency of 0.01–100 kHz under an open circuit potential of 0.24 V in dark condition. [Fe$(CN)_6]^{3-/4-}$ (5.0 mmol L^{-1}), KCl (0.1 mol L^{-1}) and phosphate buffer (adjusting the ratio of $NaH_2PO_4·2H_2O$ and $Na_2HPO_4·12H_2O$ to pH 7.0, 0.1 mol L^{-1}) were mixed and configured into the impedance solution. All experimental supplies and waste involved were disinfected with 75% alcohol to ensure the aseptic and clean detection condition.

2.2. Synthesis of Au@TiO_2 nanomaterial

TiO_2 spheres were prepared according to the previous report [33]. Concisely, ammonia solution (25.0–28.0%, 1 mL) was added into the mixture solution (EtOH: H_2O = 5: 1), and TBOT (1 mL) was added dropwise and kept stirring for 12 h at 45 °C. After centrifugation and wash, the white powder was calcined at 500 °C for 2 h under an air condition and collected as TiO_2. Au@TiO_2 nanomaterial was synthesized via one-step $C_6H_5Na_3O_7{\cdot}H_2O$ assisted reduction approach. TiO_2 powders (0.03 g) were dissolved into EtOH (30 mL). Add the prepared $HAuCl_4{\cdot}4H_2O$ (5 mg mL^{-1}, 240 μL) and $C_6H_5Na_3O_7{\cdot}H_2O$ solution (0.01 mg mL^{-1}, 2 mL) to the above solution and stir for 30 min. Followed by the centrifugation, wash, and drying in a vacuum oven (~60 °C), the nanomaterial was remarked as Au@TiO_2.

2.3. Fabrication of Nb-based PEC immunosensor

Before modification, ITO coated glass with transmittance (≥83%) and product size (10 × 10 cm^2) was cut into the area of 1 × 3 cm^2 and pretreated by ultrasonic wash with EtOH for several times. The uniformly dispersed Au@TiO_2 aqueous solution (1 mg mL^{-1}, 50 μL) was dropped to ITO electrode surface and kept dry for 30 min under an infrared lamp with a fixed area of 1 × 0.5 cm^2, named as Au@TiO_2/ITO. Nb solution (2.03 μg mL^{-1}, 10 μL) was incubated by the direct drop-coating method and stored at 4 °C for 18 h. The unabsorbed Nb was rinsed with PBS and recorded as Nb/Au@TiO_2/ITO electrode. To suppress non-specific sites, BSA solution (5 wt%, 10 μL) was dropped on the above-prepared electrode and kept for 30 min. After rinsed with PBS, the electrode was labelled as BSA/Nb/Au@TiO_2/ITO. Afterwards, drop S protein solution (10 μL) with different concentrations on the BSA/Nb/Au@TiO_2/ITO electrode and incubate it for 30 min. Followed by rinsing with PBS, SP/BSA/Nb/Au@TiO_2/ITO electrode was obtained and stored in dark at 4 °C for later detection.

3. Results and discussion

3.1. Characterization of Au@TiO_2 nanomaterial

XRD (Fig. 1A) pattern of TiO_2 shows the same shape of peaks as the standard card of anatase TiO_2 phase (JCPDS No. 99-0008), where these characteristic peaks are located at 2θ of 25.3°, 36.9°, 37.8°, 38.6°, 48.0°, 53.9°, 55.1°, 62.7°, 68.8°, 70.3°, and 75.1°. The strongest peak at 25.3° corresponds to (101) crystal face of anatase TiO_2 [34]. The diffraction peaks of Au@TiO_2 nanomaterial are the same as that of single material, illustrating that Au insertion does not change the phase behavior. Moreover, these peaks situated at 38.2°, 44.4°, 64.6°, 77.6° are corresponding to Au (JCPDS No. 99-0056), demonstrating that Au was inserted into TiO_2, and Au@TiO_2 nanomaterial was successfully synthesized without any impurities. Among these peaks, the peak at 38.2° belongs to (111) crystal face of Au. From SEM (Fig. S1) image of Au@TiO_2, it is observed spheres and the stacked nanoparticles with different sizes. From HRTEM (Fig. 1B) image of Au@TiO_2, the relative position of lattice fringes (d = 0.352 and 0.235 nm) is well in accordance with the planes of TiO_2 (101) and Au (111) separately. As observed, the agglomerated nanoparticles of Au were well grown on TiO_2 spheres. From XRD, SEM, and HRTEM results, the nanomaterial of Au nanoparticles decorated TiO_2 spheres was successfully constructed.

DRS (Fig. 1C) spectra were adopted in the ultraviolet–visible region (200–800 nm) to investigate light-absorbing capability of TiO_2 and Au@TiO_2 nanomaterial. Notably, Au@TiO_2 nanomaterial presents stronger absorbance of ultraviolet and visible light than TiO_2. TiO_2 owns the maximum absorption edge at the wavelength of ~390 nm (only the absorbance of ultraviolet light), while the absorption edge of Au@TiO_2 occurs in a red shift of ~18 nm. Au@TiO_2 has a significant enhancement in absorption of the visible region and an additional wide absorption band at ~548 nm owing to the introduction of Au [35], which can be beneficial to generating large amounts of carriers [36]. The coupling between Au and TiO_2 can effectively enhance the light utilization capability of solar energy, and the existence of Au may repress the recombination of carriers from bulk and surface of TiO_2, which can be proved by the following PEC measurements. The bandgap energy (E_g,

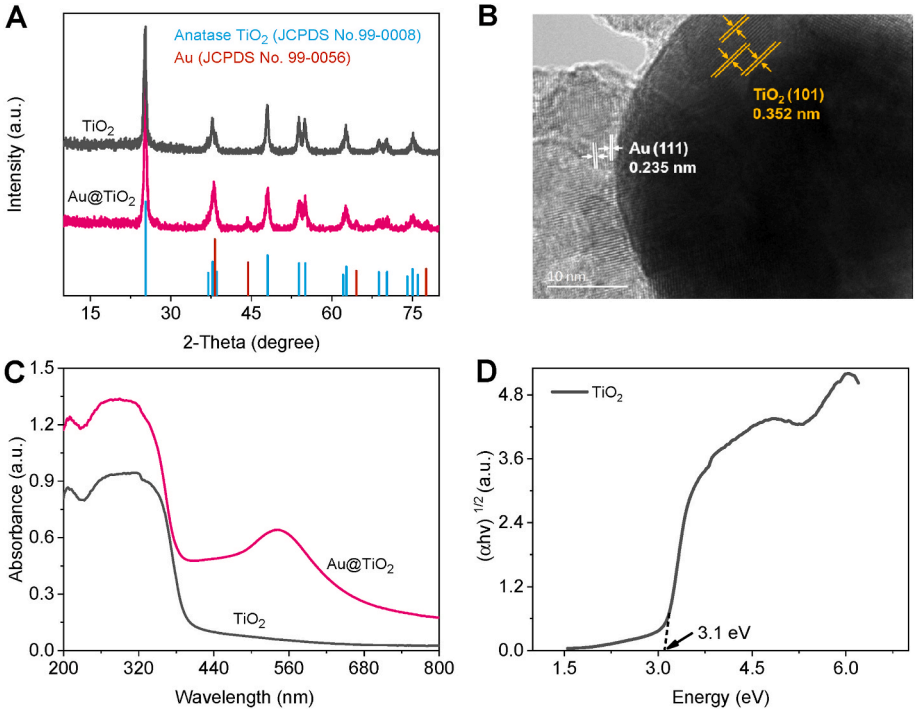

Fig. 1. XRD patterns (A) and DRS spectra (C) of TiO_2 and Au@TiO_2; (B) HRTEM image of Au@TiO_2; (D) Tauc plot of TiO_2.

Fig. 1D) was estimated by the Tauc equation of $(\alpha h\nu)^{1/2} = A\ (h\nu - E_g)$ [37]. The straight-line part of Tauc plot was extrapolated to the abscissa axis, which was E_g value (~3.1 eV) of TiO_2.

Based on DRS spectra that introducing Au nanoparticles can generate large amounts of photoinduced carriers, EIS spectra (Fig. 2A) were utilized to further verify photoelectric performance of Au@TiO_2 nanomaterial and transient photocurrent response (Fig. 2B) using AA as the electron donor for consuming photogenerated holes. The equivalent circuit diagram was inserted and simulated by ZsimpWin Software, where R_s, C_{dl}, R_{ct}, and Z_w represent solution resistance, interfacial capacitance, charge transfer resistance, and Warburg impedance, respectively (Table S1) [38]. The smaller R_{ct} value stands for the faster transfer rate of charges [39]. By comparing the measured test (dot) and calculated (solid line) data, and the error between 1.019%~2.421% of R_{ct} value, it is observed that the measured values of EIS are similar to the calculated results, demonstrating the reasonable equivalent circuit diagram. TiO_2/ITO exhibited certain R_{ct} value (~474.8 Ω) and photocurrent (~1.8 μA). After the existence of Au, the photocurrent response markedly increased to ~15.5 μA under no bias potential, which was more than 8.5 times that of TiO_2/ITO. Similarly, Au@TiO_2/ITO electrode showed small R_{ct} value (~220.6 Ω), indicating that Au@TiO_2 nanomaterial has the fast transfer efficiency of photoinduced charges. Because of the work function of Au (~5.1 eV) greater than E_g of TiO_2 [40,41], Au with SPR effect boosts transmission efficiency of photoinduced electrons to the conduction band of TiO_2 and continuing to the surface of ITO substrate through the external circuit (Fig. 4A), leading to the superior photoelectric performance.

3.2. Fabrication of Nb-based PEC immunoassay

Based on DRS characterization and PEC measurements, Au@TiO_2 nanomaterial possesses significantly enhanced PEC performance and has potential to construct a label-free PEC immunosensor as the photoelectric active material (Scheme 1). Nb of S protein, as a specific recognition agent, was effectively immobilized on the surface of Au@TiO_2 electrode owing to the Nb–Au nanoparticle conjugates with Au nanoparticles (i.e., amino or sulfhydryl group) and TiO_2 [42,43]. BSA was acted as a blocking agent to prevent Nb from decomposition and nonspecific adsorption on the electrode surface [24,29]. A Nb-based PEC immunosensor using Au@TiO_2 can be proposed, and the analysis performance for S protein can be further investigated.

Fig. 2A and B compare EIS patterns and photocurrent response with the simulated sunlight of several samples including Nb/Au@TiO_2/ITO, BSA/Nb/Au@TiO_2/ITO, and SP/BSA/Nb/Au@TiO_2/ITO electrode. After the existence of Nb, the electrode exhibited the increased R_{ct} value and the reduced photocurrent, illustrating that hindering steric effect on the electrode surface is not conducive to the transmission of photogenerated charges. Similarly, BSA/Nb/Au@TiO_2/ITO possesses lower separation and mobility ability of carriers than Nb/Au@TiO_2/ITO. When a certain concentration of S protein on the electrode was immersed (75 pg mL^{-1}, 10 μL), the increased R_{ct} value and decreased photocurrent signal (~2 μA) are observed, respectively. The immobilization of S protein on the BSA/Nb/Au@TiO_2/ITO electrode can hinder the electron transfer rate of PEC immunosensor system and to some extent obstruct electron donor (AA) to the surface reaction with the photo-induced holes, resulting in the decreased signal. Furthermore, the decrease in photocurrent response can be attributed to some electrons from AA transferred to the formed immunocomplex between Nb and S protein, causing the fast recombination rate of photoinduced electron-hole pairs. Stability test of Au@TiO_2/ITO and Nb/Au@TiO_2/ITO electrode was evaluated in PBS (pH 7.4) with 0.1 mol L^{-1} AA (Fig. 2C). After illuminating by switching the lamp at an interval of 10 s for about 36 circles, the photocurrent value almost remained no attenuation, indicating that Au@TiO_2 nanomaterial can be employed as the photoactive material for constructing a Nb-based PEC immunosensor.

3.3. Optimization of PEC immunoassay

A PEC immunoassay was constructed by employing Au@TiO_2 nanomaterial and the identification agent of Nb, and the label-free detection of S protein can be realized with high sensitivity. Based on the above measurements and analysis, S protein with Nb can occur in the immunoreaction, leading to the existence of steric hindrance effect. Before studying the analytical performance of the prepared Au@TiO_2-based PEC immunoassay, the optimization experiments were conducted for realizing highly sensitive analysis in the presence of S protein (75 pg mL^{-1}). As is Fig. 3 depicted, the concentrations of Au@TiO_2 dispersion, Nb and AA, and the incubation time of S protein on the electrode were optimized, respectively. Obviously, the photocurrent response is not positively correlated to the concentration of Au@TiO_2 dispersion (Fig. 3A). As the concentration of suspension increased (below 1 mg mL^{-1}), SP/BSA/Nb/Au@TiO_2/ITO presents a gradual increase trend in photocurrent. The increase in the concentration range from 1.0 to 1.4 mg mL^{-1} caused a slow decrease of response, which is ascribed that too high concentration becomes the recombination center of carriers of Au@TiO_2 nanomaterial [44]. The maximum photocurrent of the photoelectric active material can be beneficial to constructing the most sensitive immunosensor. Thus, the best concentration of suspension was chosen as 1.0 mg mL^{-1}.

The concentration of Nb affects the transport ability of photoinduced charges and is acted as a significant role in constructing Nb-based immunosensor (Fig. 3B). As the concentrations of Nb increased from 0.5074 to 4.06 μg mL^{-1}, photocurrent signal with 1 mg mL^{-1} suspension of Au@TiO_2 presents a trend of decrease and reached the platform at 2.03 μg mL^{-1}. The steric effect of SP/BSA/Nb/Au@TiO_2 electrode increases, and the separation ability of photoinduced carriers is suppressed to a certain extent. When the concentrations were ranging from 4.06 to 8.12 μg mL^{-1}, the photocurrent signal significantly decreased owing to the increase of steric hindrance between Nb and S protein. The obvious decrease in photocurrent signal is not conductive to the construction of PEC immunosensor for highly sensitive detection of S protein. Thus, to improve the sensitivity of immunosensor platform, the low

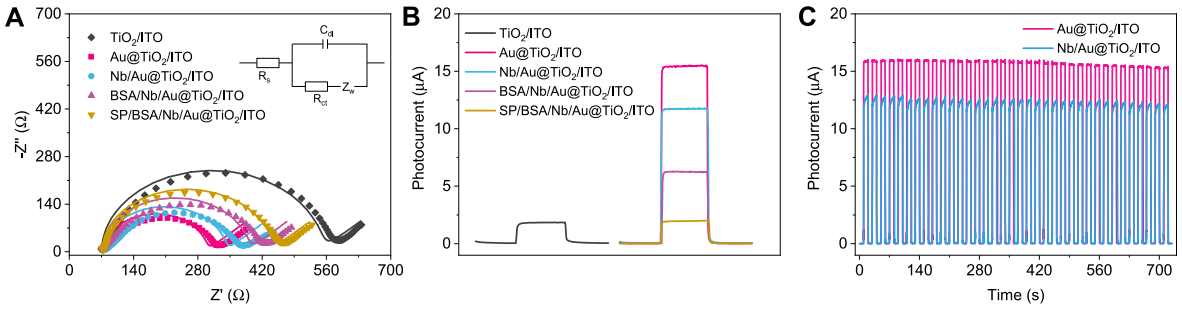

Fig. 2. EIS spectra (A, dots and solid lines represent the real test data and the corresponding fitting results, respectively) and photocurrent response (B) of different electrodes; (C) Photocurrent response of Au@TiO_2/ITO and Nb/Au@TiO_2/ITO under on-off irradiation. Inset: the equivalent circuit.

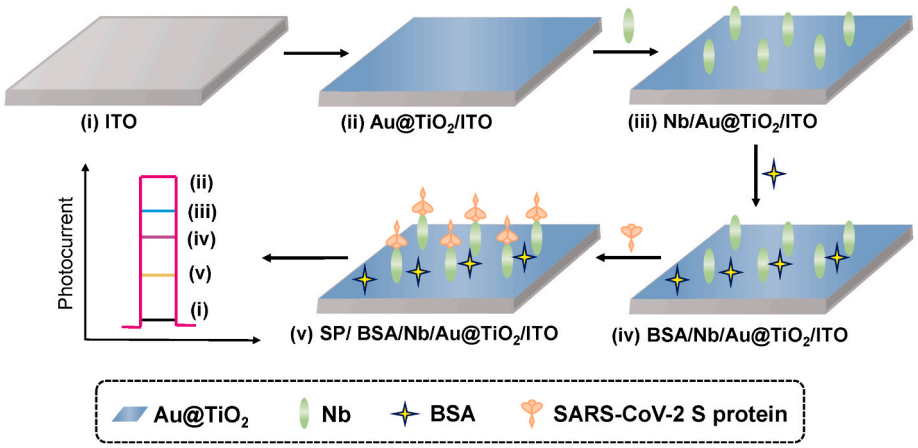

Scheme 1. Schematic construction illustration of Nb-based PEC immunoassay using Au@TiO_2 nanomaterial for detecting SARS-COV-2 S protein.

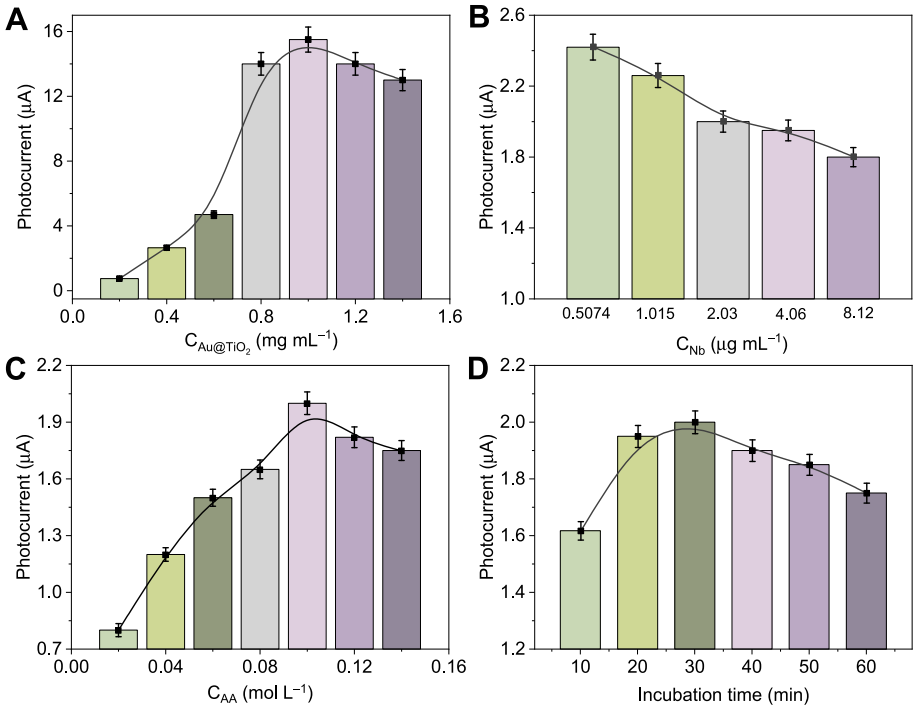

Fig. 3. Effects of the concentrations of Au@TiO_2 suspension (A), Nb (B) and AA (C), and the incubation time of S protein (D) based on SP/BSA/Nb/Au@TiO_2/ITO electrode. All photocurrent was measured in PBS with the addition of AA, and the electrode was modified with BSA (5 wt%) and S protein (75 pg mL^{-1}) from three parallel data. Error bars are equal to standard deviation (*SD*) ($n = 3$).

concentration (2.03 μg mL^{-1}) where the photocurrent reached the platform was selected as the optimal Nb concentration.

As AA concentrations increased from 0.02 to 0.1 mol L^{-1}, the photocurrent dramatically increased because AA can easily capture photogenerated holes to promote the separation of electron-hole pairs to generate photocurrent (Fig. 3C). Therefore, the recombination of electron-hole pairs can be efficiently prohibited by increasing AA concentrations, and thus the photocurrent was able to increase accordingly. However, when AA concentrations were higher than 0.1 mol L^{-1}, the photocurrent response of SP/BSA/Nb/Au@TiO_2/ITO slightly decreased because AA can retard the electron transfer between SP/BSA/Nb/Au@TiO_2/ITO and the electrode surface. Thus, 0.1 mol L^{-1} AA was selected as the optimal concentration of electron donor for PEC experiments. The more appropriate time of S protein was incubated on the electrode surface, and the more specific recognition ability of Nb can be maximized.

After the increase of the incubation time of S protein ranging from 10 to 30 min, the photocurrent decreased because S protein captured by Nb increases with time increasing, the steric hindering on the electrode surface increases by the immunoreaction of Nb and S protein (Fig. 3D). The photocurrent maximum was achieved for S protein with the incubation time of 30 min. Thus, the optimality of immersion time was selected as 30 min. A PEC immunoassay was optimized using Au@TiO_2 suspension (~1.0 mg mL^{-1}), Nb (~2.03 μg mL^{-1}), AA (0.1 mol L^{-1}), and immersion time (~30 min) for S protein detection.

3.4. PEC immunoassay of SARS-CoV-2 S protein

Under the optimal parameters, this Nb-based PEC immunosensor was used for detecting the S protein, and the analysis performance was investigated in Fig. 4B and C. The photocurrent value presents the gradual decrease with the increase of S protein in the concentration

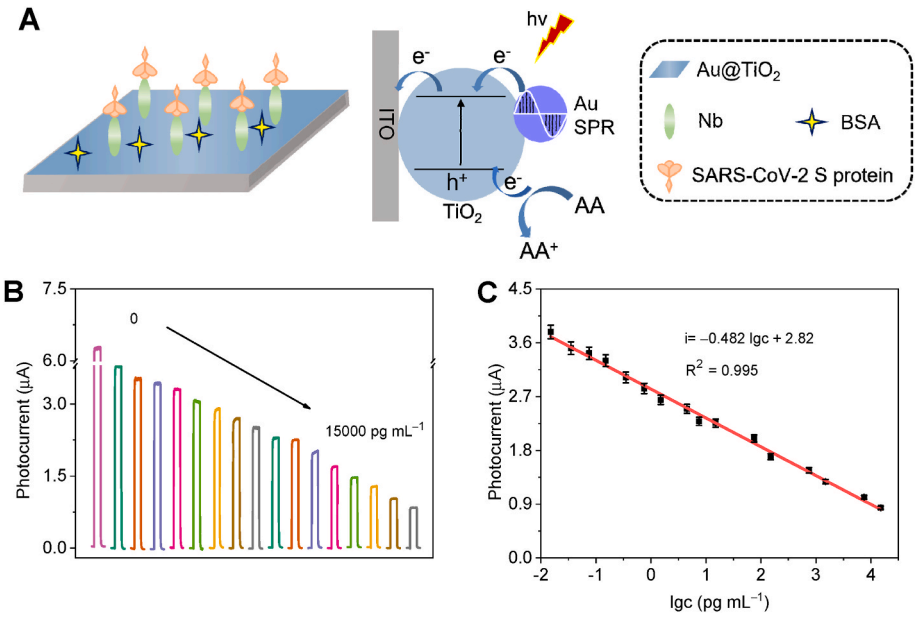

Fig. 4. (A) Mechanism diagram for the determination of S protein by Au@TiO_2-based on PEC immunosensor; (B) Photocurrent response of PEC immunoassay upon different concentrations of S protein: 0, 0.015, 0.035, 0.075, 0.15, 0.35, 0.75, 1.5, 4.5, 7.5, 15, 75, 150, 750, 1500, 7500, 15000 pg mL^{-1}; (C) Linear curve. Data were obtained from three parallel measurements, and error bars are equal to *SD* ($n = 3$).

range of 0.015 (Fig. 4B) to 15000 pg mL^{-1}. Furthermore, the regression equation between the logarithm of S protein concentration (lgc) and photocurrent response (i) obtained by the linear fitting was $i = -0.482$ lgc+2.82 by three independent and parallel tests (Fig. 4C, detection range: 0.015–15000 pg mL^{-1}) with a high linear correlation ($R^2 = 0.995$). When the signal-to-noise ratio (S/N) is 3, LOD was calculated to be 5 fg mL^{-1}, where S and N represent the measured value of three parallel photocurrent and the slope of the standard curve separately. The label-free PEC immunosensor based on Au@TiO_2 achieved the sensitive determination for SARS-CoV-2 S protein, which can attribute to the following three reasons: (i) the introduction of Au with SPR effect boosts the effective transmission efficiency of photoinduced electrons, leading to the superior photoelectric conversion efficiency; (ii) Nb with the disulfide bond can facilitate the immobilization with Au nanoparticles to form a gold-thiolate bond of Nb–Au nanoparticle conjugates; (iii) Nb with high affinity bound to S protein to trigger the immunoreaction, resulting in a subsequent formation of the immunocomplex on the sensing interface.

By comparing the reported methods (Table 1) for detecting S protein of SARS-CoV-2, opto-microfluidic chip, phononic and field-effect transistor (FET) sensors realized the rapid analysis and exhibited high sensitivity, but limited in the disadvantages of relatively expensive spectrometer and high fabrication cost. In this work, the Nb-based PEC immunoassay platform is highly sensitive and label-free, which can significantly reduce the assay time and consequently the overall assay cost. However, the current platform is still at proof-of-concept stage and difficult to realize real-time monitoring of real sample. Our future work aims to collaborate with local hospitals to perform assays with real COVID-19 patient sample to validate and compare the true performance with the existing serological Nb assays.

To confirm the selectivity of BSA/Nb/Au@TiO_2/ITO electrode to SARS-CoV-2 S protein, the immunosensor was tested by incubating the target S protein (75 pg mL^{-1}) against several inferring substances (7.5 ng mL^{-1}) such asuric acid, L-lysine, L-glutamic acid, and their mixture. The mixture was obtained by mixing each interference substances at 100 times with S protein, respectively. Fig. 5A shows no or insignificant inference effect in photocurrent response of the PEC immunosensor against interfering substances compared with that of SARS-CoV-2 S protein. Furthermore, based on the selective experiments by Gai and coworkers [32], it is found that Nb can selectively integrate with the mutants of SARS-CoV-2, illustrating that Nb has the selective ability for inhibiting the interaction between ACE2 and receptor-binding domain

Table 1
Comparison of different biosensors for detecting SARS-CoV-2 S protein.

Biosensor	Method	LOD (fg mL^{-1})	Advantages	Disadvantages	Ref.
Opto-microfluidic sensor	Microfluidic device with Au nanospikes	8.0×10^4	Compact device and fast detection (30 min)	High operator requirements	[45]
Phononic sensor	Antibody-coupled graphene	1.0	Real-time detection and low fabrication cost	Relatively expensive spectrometer	[46]
FET sensor	Graphene-based device	1.0	Real-time detection and quick analysis	High fabrication and testing cost	[11]
FET sensor	Semiconducting single-walled carbon nanotube with antibody	0.55	Rapid detection (5 min) and high sensitivity	High fabrication and testing cost	[47]
Electrochemical immunosensor	Label-free detection	1.0×10^2	Low immunological response time (5 min) and easy preparation	Low stability	[48]
Electrochemical immunosensor	Magnetic bead-based screen-printed carbon electrodes	1.9×10^7	Rapid analysis (30 min) and portable instrument	Low stability	[16]
PEC immunosensor	Label-free detection	5.0	Simple operation, rapid response (30 min) and low cost	Difficult to real-time detection	This work

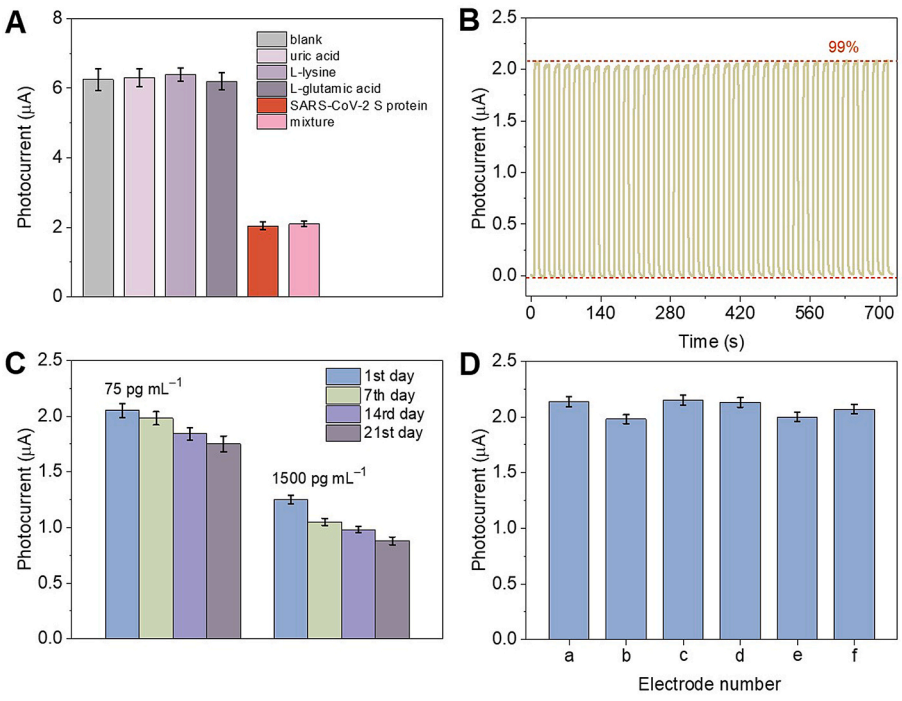

Fig. 5. (A) Photocurrent response of BSA/Nb/Au@TiO_2/ITO towards incubating 75 pg mL^{-1} S protein and 7.5 ng mL^{-1} interference substances and their mixture; (B) Photocurrent response by PEC immunoassay in the presence of S protein under on-off irradiation; (C) Long-stability of PEC immunoassay with S protein of 75 and 1500 pg mL^{-1}; (D) Reproducibility of PEC immunoassay with six electrodes in parallel. Data were obtained from three parallel measurements, and error bars are equal to *SD* ($n = 3$).

of S protein. After signal on-off irradiation for 36 circles around 700 s (at 10 s intervals, Fig. 5B), the photocurrent value had almost no attenuation and still maintained the initial 99% in the presence of 75 pg mL^{-1} S protein. The photocurrent of Nb/Au@TiO_2/ITO electrode with concentrations of 75 pg mL^{-1} and 1500 pg mL^{-1} S protein stored in dark at 4 °C for 21 days was tested (Fig. 5C). After the long-term storage, the immunosensor possessed less signal attenuation, indicating exceptional stability of this fabricated sensor. Fig. 5D shows the reproducibility of six BSA/Nb/Au@TiO_2/ITO electrodes with the immersed 75 pg mL^{-1} S protein by the same modification. Compared to the standard photocurrent value (~2.08 μA), the relative standard deviation (RSD) was below 4%, demonstrating high reproducibility by this prepared PEC immunosensor.

Based on the linear equation of PEC immunoassay, the applicability for the detection of SARS-CoV-2 S protein was investigated in oropharyngeal swab sample. The sample from healthy/normal individuals were kept at −80 °C until further use. For the detection, the sample was diluted 1:10 in PBS with the addition of AA (Table S2). Recovery with S protein (6 pg mL^{-1}) was calculated to be 99.83%, and RSD value was 1.04%. This proves that this prepared Nb-based PEC immunosensor can be great potential to determine the concentration of S protein determination to be tested, and the success of the platform to detect the virus protein with high accuracy and without significant interference from oropharyngeal swab sample.

4. Conclusion

A Nb-based PEC immunoassay using Au@TiO_2 nanomaterial was put forward for label-free determination of SARS-CoV-2 S protein. Au nanoparticles were well grown on TiO_2 sphere, named as Au@TiO_2 nanomaterial. SPR effect of Au nanoparticles can greatly boost the nanomaterial with stronger visible light harvesting, faster transmission efficiency of photoinduced charges and better photoelectric signal than TiO_2. This constructed Nb-based PEC immunosensor of S protein realized with satisfactory sensitivity, stability, reproducibility, and applicability. This design can provide a new way for fabricating the immunosensor based on nanobody and opens the monitoring of COVID-19 virus with a simple and fast PEC immunoassay.

CRediT authorship contribution statement

Yun Chen: Formal analysis, Writing – original draft. **Wei Duan:** Investigation, Writing – original draft. **Li Xu:** Methodology, Formal analysis. **Guanghui Li:** Methodology, Formal analysis. **Yakun Wan:** Conceptualization, Resources. **Henan Li:** Supervision, Writing – review & editing.

Declaration of competing interest

The authors declare the following financial interests/personal relationships which may be considered as potential competing interests: All commercial rights from this paper belong to Shanghai Novamab Biopharmaceuticals Co., Ltd.

Acknowledgements

This work has been financially supported by High-tech Research Key Laboratory of Zhenjiang (SS2018002), Jiangsu Province Key Laboratory of Intelligent Building Energy Efficiency (BEE201904), a Project Funded by the Priority Academic Program Development of Jiangsu Higher Education Institutions, and Science Foundation of Jiangsu Province (BK20180971, BK20180103).

Appendix A. Supplementary data

Supplementary data to this article can be found online at https://doi.org/10.1016/j.aca.2022.339904.

References

[1] S. Eissa, M. Zourob, Development of a low-cost cotton-tipped electrochemical immunosensor for the detection of SARS-CoV-2, Anal. Chem. 93 (2021) 1826–1833.
[2] C.L. Huang, Y.M. Wang, X.W. Li, L.L. Ren, J.P. Zhao, Y. Hu, L. Zhang, G.H. Fan, J. Y. Xu, X.Y. Gu, Z.S. Cheng, T. Yu, J.A. Xia, Y. Wei, W.J. Wu, X.L. Xie, W. Yin, H. Li, M. Liu, Y. Xiao, H. Gao, L. Guo, J.G. Xie, G.F. Wang, R.M. Jiang, Z.C. Gao, Q. Jin, J. W. Wang, B. Cao, Clinical features of patients infected with 2019 novel coronavirus in Wuhan, China, Lancet 395 (2020) 497–506.
[3] A.C. Marques, T. Pinheiro, M. Morais, C. Martins, A.F. Andrade, R. Martins, M.G. F. Sales, E. Fortunato, Bottom-up microwave-assisted seed-mediated synthesis of

gold nanoparticles onto nanocellulose to boost stability and high performance for SERS applications, Appl. Surf. Sci. 561 (2021), 150060.
[4] J.Z. Shi, Z.Y. Wen, G.X. Zhong, H.L. Yang, G. Wang, B.Y. Huang, R.Q. Liu, X.J. He, L. Shuai, Z.R. Sun, Y.B. Zhao, P.P. Liu, L.B. Liang, P.F. Cui, J.L. Wang, X.F. Zhang, Y.T. Guan, W.J. Tan, G.Z. Wu, H.L. Chen, Z.G. Bu, Susceptibility of ferrets, cats, dogs, and other domesticated animals to SARS-coronavirus 2, Science 368 (2020) 1016–1020.
[5] S. Eissa, M. Zourob, Development of a low-cost cotton-tipped electrochemical immunosensor for the detection of SARS-CoV-2, Anal. Chem. 93 (2021) 1826–1833.
[6] E. Sheikhzadeh, S. Eissa, A. Ismail, M. Zourob, Diagnostic techniques for COVID-19 and new developments, Talanta 220 (2020), 121392.
[7] A. Bernheim, X. Mei, M. Huang, Y. Yang, Z.A. Fayad, N. Zhang, K. Diao, B. Lin, X. Zhu, K. Li, S. Li, H. Shan, A. Jacobi, M. Chung, Chest CT findings in coronavirus disease-19 (COVID-19): relationship to duration of infection, Radiology 295 (2020), 200463.
[8] M.R. Eguilaz, L.R. Cumba, R.J. Forster, Electrochemical detection of viruses and antibodies: a mini review, Electrochem. Commun. 116 (2020) 106762.
[9] W. Zhang, R.H. Du, B. Li, X.S. Zheng, X.L. Yang, B. Hu, Y.Y. Wang, G.F. Xiao, B. Yan, Z.L. Shi, P. Zhou, Molecular and serological investigation of 2019-nCoV infected patients: implication of multiple shedding routes, Emerg. Microb. Infect. 9 (2020) 386–389.
[10] A. Idili, C. Parolo, R. Alvarez-Diduk, A. Merkoci, Rapid and efficient detection of the SARS-CoV-2 spike protein using an electrochemical aptamer-based sensor, ACS Sens. 6 (2021) 3093–3101.
[11] G. Seo, G. Lee, M.J. Kim, S.H. Baek, M. Choi, K.B. Ku, C.S. Lee, S. Jun, D. Park, H. G. Kim, S.J. Kim, J.O. Lee, B.T. Kim, E.C. Park, S.I. Kim, Rapid detection of COVID-19 causative virus (SARS-CoV-2) in human nasopharyngeal swab specimens using field-effect transistor-based biosensor, ACS Nano 14 (2020) 5135–5142.
[12] H. Yousefi, A. Mahmud, D.R. Chang, J. Das, S. Gomis, J.B. Chen, H.S. Wang, T. Been, L. Yip, E. Coomes, Z.J. Li, S. Mubareka, A. McGeer, N. Christie, S. Gray-Owen, A. Cochrane, J.M. Rini, E.H. Sargent, S.O. Kelley, Detection of SARS-CoV-2 viral particles using direct, reagent-free electrochemical sensing, J. Am. Chem. Soc. 143 (2021) 1722–1727.
[13] X.C. Liao, X. Wang, M.M. Zhang, L.S. Mei, S.Y. Chen, Y. Qi, C.L. Hong, An immunosensor based on an electrochemical-chemical-chemical advanced redox cycle amplification strategy for the ultrasensitive determination of CEA, Anal. Chim. Acta 1170 (2021), 338647.
[14] Z.Y. Wang, S.F. Zong, L. Wu, D. Zhu, Y.P. Cui, SERS-activated platforms for immunoassay: probes, encoding methods, and applications, Chem. Rev. 117 (2017) 7910–7963.
[15] H. Zhao, F. Liu, W. Xie, T.C. Zhou, J. OuYang, L. Jin, H. Li, C.Y. Zhao, L. Zhang, J. Wei, Y.P. Zhang, C.P. Li, Ultrasensitive supersandwich-type electrochemical sensor for SARS-CoV-2 from the infected COVID-19 patients using a smartphone, Sensor. Actuator. B Chem. 327 (2021), 128899.
[16] L. Fabiani, M. Saroglia, G. Galata, R.D. Santis, S. Fillo, V. Luca, G. Faggioni, N. D'Amore, E. Regalbuto, P. Salvatori, G. Terova, D. Moscone, F. Lista, F. Arduini, Magnetic beads combined with carbon black-based screen-printed electrodes for COVID-19: a reliable and miniaturized electrochemical immunosensor for SARS-CoV-2 detection in saliva, Biosens. Bioelectron. 171 (2021), 112686.
[17] H. Chen, S.G. Park, N. Choi, H.J. Kwon, T. Kang, M.K. Lee, J. Choo, Sensitive detection of SARS-CoV-2 using a SERS-based aptasensor, ACS Sens. 6 (2021) 2378–2385.
[18] R.L. Pinals, F. Ledesma, D. Yang, N. Navarro, S. Jeong, J.E. Pak, L. Kuo, Y. C. Chuang, Y.W. Cheng, H.Y. Sun, M.P. Landry, Rapid SARS-CoV-2 spike protein detection by carbon nanotube based near-infrared nanosensors, Nano Lett. 21 (2021) 2272–2280.
[19] N. Gao, Y.F. Zhang, K.K. Gao, J.D. Xie, L. Liu, Y.Y. Li, L.P. Qiu, Q. Wei, H.M. Ma, X. H. Pang, Ultrasensitive label-free photoelectrochemical immunosensor for the detection of amyloid beta-protein based on Zn:SnO_2/SnS_2-Au nanocomposites, Sensor. Actuator. B Chem. 308 (2020), 127576.
[20] G.J. Chen, Y. Qin, L. Jiao, J.J. Huang, Y. Wu, L.Y. Hu, W.L. Gu, D.C. Xu, C.Z. Zhu, Nanozyme-activated synergistic amplification for ultrasensitive photoelectrochemical immunoassay, Anal. Chem. 93 (2021) 6881–6888.
[21] K.Y. Chen, J.Y. Xue, Q. Zhou, Y. Zhang, M.M. Zhang, Y.J. Zhang, H. Zhang, Y. F. Shen, Coupling metal-organic framework nanosphere and nanobody for boosted photoelectrochemical immunoassay of Human Epididymis Protein 4, Anal. Chim. Acta 1107 (2020) 145–154.
[22] X.Y. Yu, Q.L. Xu, Y. Wu, H.J. Jiang, W. Wei, A. Zulipikaer, Y. Guo, Jirimutu, J. Chen, Nanobodies derived from camelids represent versatile biomolecules for biomedical applications, Biomater. Sci. 8 (2020) 3559–3573.
[23] T. De Meyer, S. Muyldermans, A. Depicker, Nanobody-based products as research and diagnostic tools, Trends Biotechnol. 32 (2014) 263–270.
[24] H.N. Li, Y.W. Mu, J.R. Yan, D.M. Cui, W.J. Ou, Y.K. Wan, S.Q. Liu, Label-free photoelectrochemical immunosensor for neutrophil gelatinase-associated lipocalin based on the use of nanobodies, Anal. Chem. 87 (2015) 2007–2015.
[25] Q. Zhou, G.H. Li, Y.J. Zhang, M. Zhu, Y.K. Wan, Y.F. Shen, Highly selective and sensitive electrochemical immunoassay of Cry1C using nanobody and π-π stacked graphene oxide/thionine assembly, Anal. Chem. 88 (2016) 9830–9836.
[26] M.A. Rossotti, M. Pirez, A. Gonzalez-Techera, Y. Cui, C.S. Bever, K.S.S. Lee, C. Morisseau, C. Leizagoyen, S. Gee, B.D. Hammock, G. González-Sapienza, Method for sorting and pairwise selection of nanobodies for the development of highly sensitive sandwich immunoassays, Anal. Chem. 87 (2015) 11907–11914.
[27] D.Y. Li, C. Morisseau, C.B. McReynolds, T. Duflot, J. Bellien, R.M. Nagra, A. Y. Taha, B.D. Hammock, Development of improved double-nanobody sandwich ELISAs for human soluble epoxide hydrolase detection in peripheral blood mononuclear cells of diabetic patients and the prefrontal cortex of multiple sclerosis patients, Anal. Chem. 92 (2020) 7334–7342.
[28] S. Muyldermans, Nanobodies: natural single-domain antibodies, Annu. Rev. Biochem. 82 (2013) 775–797.
[29] D.P. Rao, K.N. Mei, T.H. Yan, Y. Wang, W.J. Wu, Y. Chen, J.Y. Wang, Q.C. Zhang, S. Q. Wu, Nanomechanical sensor for rapid and ultrasensitive detection of tumor markers in serum using nanobody, Nano Res. 152 (2021) 1–10.
[30] M. Dumoulin, K. Conrath, A. Van Meirhaeghe, F. Meersman, K. Heremans, L. G. Frenken, S. Muyldermans, L. Wyns, A. Matagne, Single-domain antibody fragments with high conformational stability, Protein Sci. 11 (2002) 500–515.
[31] X. Liu, Y.P. Wen, W.J. Wang, Z.T. Zhao, Y. Han, K.J. Tang, D. Wang, Nanobody-based electrochemical competitive immunosensor for the detection of AFB1 through AFB1-HCR as signal amplifier, Microchim. Acta 187 (2020) 352.
[32] J.W. Gai, L.L. Ma, G.H. Li, M. Zhu, P. Qiao, X.F. Li, H.W. Zhang, Y.M. Zhang, Y. D. Chen, W.W. Ji, H. Zhang, H.H. Cao, X.H. Li, R. Gong, Y.K. Wan, A potent neutralizing nanobody against SARS-CoV-2 with inhaled delivery potential, MedComm 2 (2021) 1–13.
[33] W. Li, J.P. Yang, Z.X. Wu, J.X. Wang, B. Li, S.S. Feng, Y.H. Deng, F. Zhang, D. Y. Zhao, A versatile kinetics-controlled coating method to construct uniform porous TiO_2 shells for multifunctional core-shell structures, J. Am. Chem. Soc. 134 (2012) 11864–11867.
[34] F. He, A.Y. Meng, B. Cheng, W.K. Ho, J.G. Yu, Enhanced photocatalytic H_2-production activity of WO_3/TiO_2 step-scheme heterojunction by graphene modification, Chinese J. Catal. 41 (2020) 9–20.
[35] M.J. Li, S.Y. An, Y. Wu, Photoelectrochemical monitoring of miRNA based on Au NPs@g-C_3N_4 coupled with exonuclease-involved target cycle amplification, Anal. Chim. Acta 1187 (2021), 339156.
[36] J.T. Dong, F. Chen, L. Xu, P.C. Yan, J.C. Qian, Y. Chen, M.Y. Yang, H.N. Li, Fabrication of sensitive photoelectrochemical aptasensor using Agnanoparticles sensitized bismuth oxyiodide for determinationof chloramphenicol, Microchem. J. 178 (2022) 107317.
[37] X.W. Zhu, Z.L. Wang, K. Zhong, Q.D. Li, P.H. Ding, Z.Y. Feng, J.M. Yang, Y.S. Du, Y. H. Song, Y.J. Hua, J.J. Yuan, Y.B. She, H.M. Li, H. Xu, Mo-O-Bi bonds as interfacial electron transport bridges to fuel CO_2 photoreduction via in-situ reconstruction of black Bi_2MoO_6/BiO_{2-x} heterojunction, Chem. Eng. J. 429 (2022), 132204.
[38] X.W. Zhu, S.Q. Huang, Q. Yu, Y.B. She, J.M. Yang, G.L. Zhou, Q.D. Li, X.J. She, J. J. Deng, H.M. Li, H. Xu, In-situ hydroxyl modification of monolayer black phosphorus for stable photocatalytic carbon dioxide conversion, Appl. Catal. B Environ. 269 (2020), 118760.
[39] X.W. Zhu, J.M. Yang, X.L. Zhu, J.J. Yuan, M. Zhou, X.J. She, Q. Yu, Y.H. Song, Y. B. She, Y.J. Hua, H.M. Li, H. Xu, Exploring deep effects of atomic vacancies on activating CO_2 photoreduction via rationally designing indium oxide photocatalysts, Chem. Eng. J. 422 (2021), 129888.
[40] C. Fu, M.J. Li, H.J. Li, C.P. Li, X. Guo Wu, B.H. Yang, Fabrication of Au nanoparticle/TiO_2 hybrid films for photoelectrocatalytic degradation of methyl orange, J. Alloys Compd. 692 (2017) 727–733.
[41] X. He, Y. Guo, X. Li, J.H. Liu, Light harvesting enhancement by hierarchical Au/TiO_2 microspheres consisted with nanorod units for dye sensitized solar cells, Sol. Energy 207 (2020) 592–598.
[42] D.A. Richards, A. Maruani, V. Chudasama, Antibody fragments as nanoparticle targeting ligands: a step in the right direction, Chem. Sci. 8 (2017) 63–77.
[43] H. Wang, G.H. Li, Y.H. Zhang, M. Zhu, H.M. Ma, B. Du, Q. Wei, Y.K. Wan, Nanobody-based electrochemical immunoassay for ultrasensitive determination of apolipoprotein-A1 using silver nanoparticles loaded nanohydroxyapatite as label, Anal. Chem. 87 (2015) 11209–11214.
[44] Y. Chen, M. Yang, Y. Jia, P. Yan, F. Chen, J. Qian, L. Xu, H. Li, NiS_2/NiFe LDH/g-C_3N_4 ternary heterostructure-based label-free photoelectrochemical aptasensing for highly sensitive determination of enrofloxacin, Mater. Today Chem. 24 (2022), 100845.
[45] R. Funari, K.Y. Chu, A.Q. Shen, Detection of antibodies against SARS-CoV-2 spike protein by gold nanospikes in an opto-microfluidic chip, Biosens. Bioelectron. 169 (2020), 112578.
[46] N.H.L. Nguyen, S. Kim, G. Lindemann, V. Berry, COVID-19 spike protein induced phononic modification in antibody-coupled graphene for viral detection application, ACS Nano 15 (2021) 11743–11752.
[47] W.T. Shao, M.R. Shurin, S.E. Wheeler, X.Y. He, A. Star, Rapid detection of SARS-CoV-2 antigens using high-purity semiconducting single-walled carbon nanotube-based field-effect transistors, ACS Appl. Mater. Interfaces 13 (2021) 10321–10327.
[48] M. Mehmandoust, Z.P. Gumus, M. Soylak, N. Erk, Electrochemical immunosensor for rapid and highly sensitive detection of SARS-CoV-2 antigen in the nasal sample, Talanta 240 (2022), 123211.